Hut78 and mutants

As seen in the introduction, the structure of the protein Hut78 results from the fusion of the first 666 amino acids of p100, fused to three extra amino acids, serine-alanine-serine (SAS) (Thakur *et al*., 1994; Zhang *et al*., 1994). It maintains therefore the N-terminal part of p100, containing the Rel homology domain (RHD) with its nuclear localization signal (NLS), the glycine rich region (GRR) involved in the processing into p52 and five of the seven ankyrin repeats, but it lacks the C-terminal processing inhibitory domain (PID). In order to determine the functional domains of Hut78 involved in its oncogenic activity, we mutated or deleted the principal regions of the protein and observed the effects of such alterations on the properties of Hut78. The different mutants generated and tested in this work, are listed here and represented in **figure 17**:

♦ ***Hut78***: the Hut78 protein was previously cloned in our laboratory from the p100 template using a 3' primer with an additional sequence encoding the three extra amino acids SAS (Gaëtan Vanstraelen, Patrick Viatour).

♦ ***NLS1234***: this mutant was obtained by site-directed mutagenesis targeting the amino acids of the predicted nuclear localization signal (RKRRK).

♦ ***ΔGRR***: deletion of the glycine-rich region, required for the processing of Hut78 into p52 (Lin and Ghosh, 1996), results in a mutant that doesn't generate p52 anymore.

♦ ***K75A***: Michalopoulos and Hay identified the lysine 80 of p50 for its binding to DNA and for the stabilization of the DNA-protein complex (Michalopoulos and Hay, 1999). This lysine residue is highly conserved among all the Rel/NF-κB proteins, except in c-Rel, where there is an arginine instead of a lysine, suggesting that the interaction is due to the positive charge of the amino acid. The authors showed that replacement of this positively charged hydrophilic lysine with alanine did not change the overall structure of p50 dimers (Cramer *et al*., 1997; Michalopoulos and Hay, 1999). By structure analogy, we determined that the lysine 75 in p52 corresponds to the lysine 80 in p50, and as p52 loop has a very similar structure to its p50 homologue, we also chose to mutate this residue in alanine, by site-directed mutagenesis.

♦ ***ankyrin mutants***: these different C-terminally truncated Hut78 mutants were generated by insertion of a stop codon after each ankyrin repeat and thus retain from 1 (ankyrin 1) to 5 (ankyrin 5) ankyrin repeats.

♦ ***RHD mutants***: these N-terminally truncated Hut78 mutants were generated by PCR and lack variable portions of the Rel Homology domain (RHD).

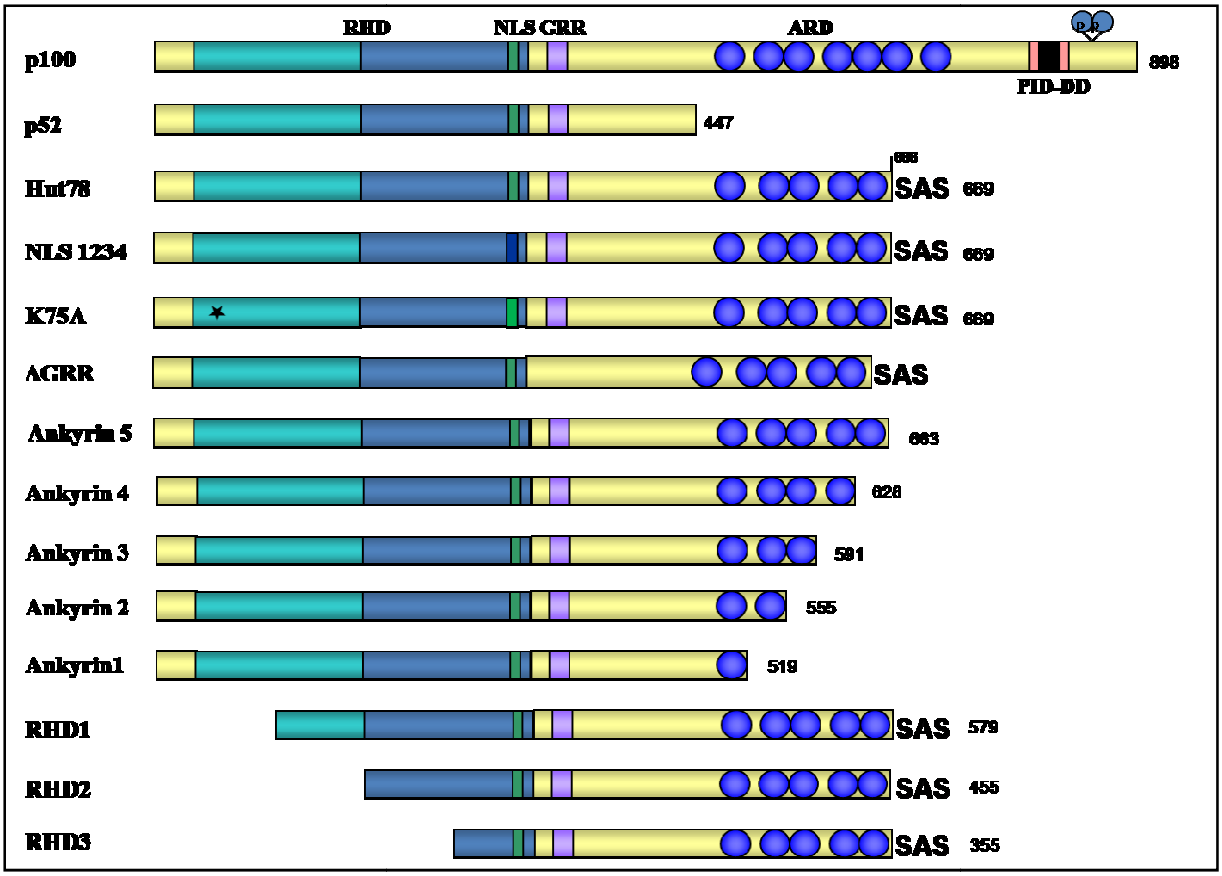

Figure 17: Schematic representation of the different Hut78 mutants generated in this work. They lack, after deletion or mutation, variable portions of the principal functional domains of the protein, including the Rel Homology domain (RHD), the ankyrin-repeats domain (ARD), the nuclear localization signal (NLS) or the glycine-rich region (GRR). The star in K75A mutant represents the lysine in position 75, mutated in alanine. The number of amino acids of each protein is indicated on the right.

Determination of the subcellular localization of Hut78

Nuclear extracts immunoblottings and immunofluorescence assays in the HUT78 cell line, previously shown that both p52 and Hut78 are located in the nucleus, suggesting that Hut78 can translocate into the nucleus as a primary translation product, without further proteolytic processing (Thakur *et al*., 1994; Zhang *et al*., 1994). To confirm the nuclear localization of Hut78, we performed an immunofluorescence assay in HeLa cells overexpressing p100, p52 or FLAG-Hut78, using a primary antibody targeting the common N-terminal part of these proteins and a secondary antibody coupled to FITC (**Figure 18**).

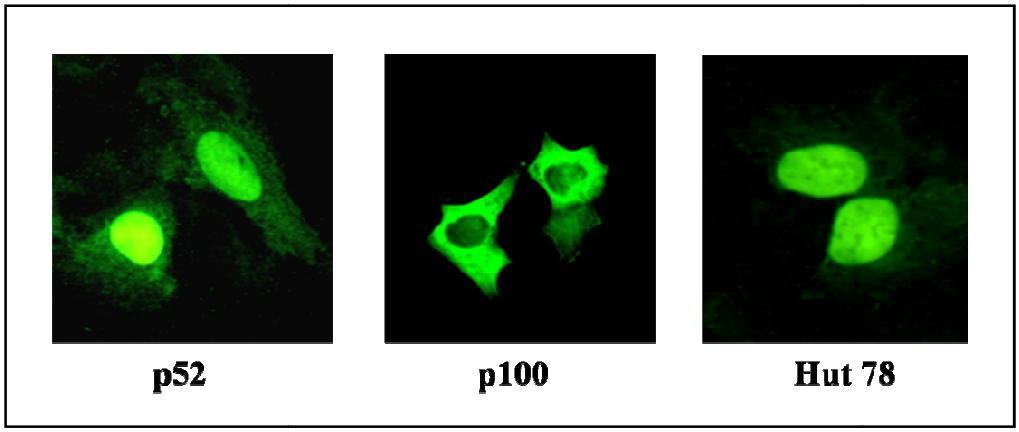

Figure 18: Hut78 is localized in the nucleus like p52, whereas p100 remains in the cytoplasm. HeLa cells were transfected with 2µg of the indicated expression vectors and analyzed by immunofluorescence using an antiserum recognizing the N-terminal peptide of NF-κB2 p52/p100 as a primary antibody and FITC-conjugate anti-mouse IG as secondary antibody.

We observed that p52 and Hut78 are found in the nucleus, whereas p100 remains in the cytoplasm. Taken together, these results suggest that loss of the C-terminal domain of p100 alters the subcellular localization of the protein and allows it to escape the regulatory mechanisms which retain p100 in the cytoplasm. Deletion of the death domain (DD) and/or ankyrin repeats disrupts the three-dimensional domain formed by C- and N-terminal sequences interaction, making the NLS exposed, which results in the nuclear translocation of the protein (Qing *et al*., 2005a). Moreover, the C-terminal part of p100 was shown to possess a nuclear export function, which could also partly explain the nuclear localization of the truncated mutants lacking this region (Solan *et al*., 2002).

The putative nuclear localization signal identified in p50, p65 and c-rel (Gilmore and Temin 1988; Hannink and Temin, 1989) was shown to be conserved in the protein sequence of NF-κB2/p100 (Neri *et al*., 1991). This sequence is composed of five basic, positively charged amino acids (RKRRK), located in the C-terminal part of the Rel Homology domain (amino acids 337 to 341). To prove the critical role of this sequence in the nuclear import of the truncated NF-κB2 protein Hut78, we next generated from one (NLS1 to NLS5) to four amino acids substitutions (NLS 1234) within the NLS sequence and subsequently addressed the localization of the resulting Hut78 mutants by immunofluorescence (**Figure 19**).

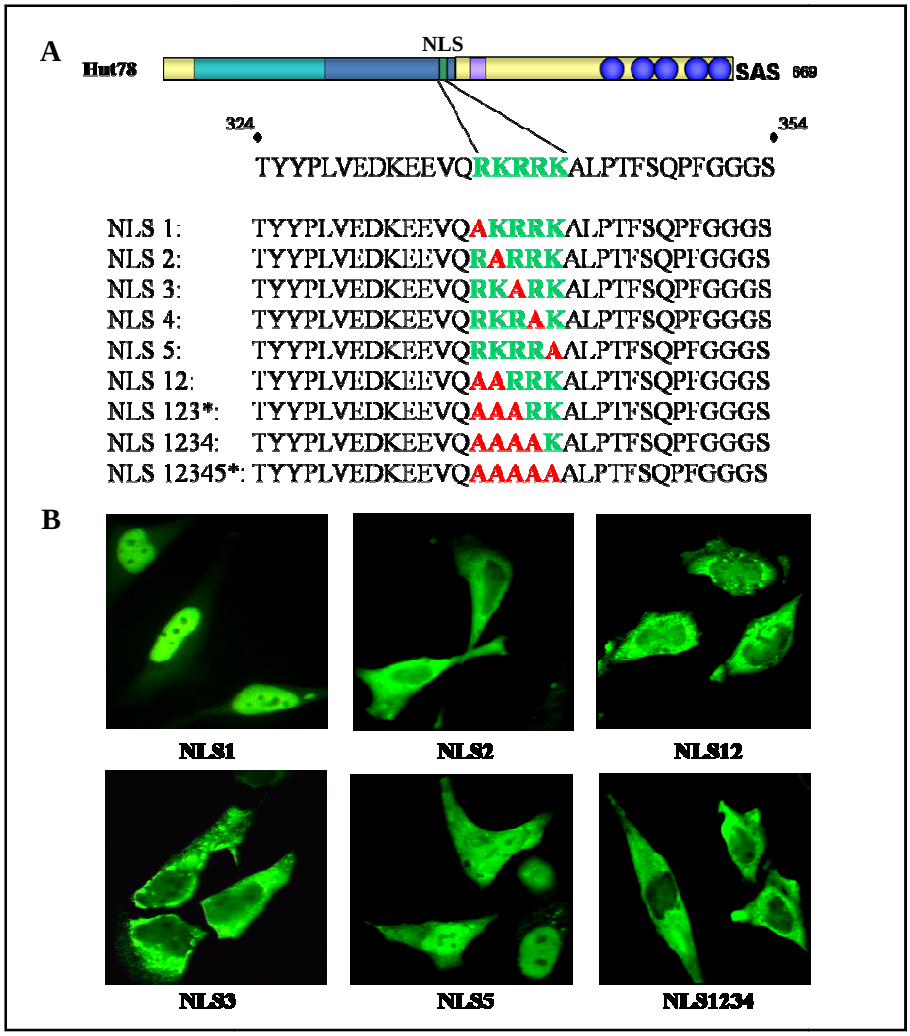

Figure 19: The nuclear localization of Hut78 requires a functional NLS located within the RHD domain. (A) Schematic representation of the truncated NF-κB2 protein Hut78 and mutants harboring from 1 ("NLS 1" to "NLS 5") to 4 lysine to alanine substitutions ("NLS 1234") within the nuclear localization sequence ("NLS") which spans from amino acids 337 to 341 (green letters). The red letters indicate the point mutations introduced. *Mutants non generated **(B)** HeLa cells were transfected with 2µg of the indicated expression vectors and analyzed by immunofluorescence using an antiserum recognizing the N-terminal peptide of NF-κB2/p100 as a primary antibody and FITC-conjugate anti-mouse IG as secondary antibody.

We observed that mutation of the amino acids 337 (R) and 341 (K) had no or little effect on the localization of the protein Hut78, as mutants NLS1 and NLS5 were still nuclear. In contrast, mutants NLS2 and NLS3 were mostly found in the cytoplasm, suggesting that amino acids 338 (K) and 339 (R) are essential for the nuclear localization of Hut78. Mutation of four amino acids, 337 to 340, generates a mutant, NLS1234, which is fully cytoplasmic.

Recently, Xiao and colleagues proposed a mechanism to explain the constitutive processing of p100 C-terminally truncated mutants (p100ΔCs): deletion of the C-terminal PID and/or ankyrin repeats of p100 leads to the translocation of the p100ΔC proteins into the nucleus and subsequent recruitment of the proteasome to form a stable complex proteasome/p100ΔC/DNA at a κB promoter, responsible for the processing of p100ΔCs (Qing *et al*., 2007). They showed that direct binding of p100ΔCs to the κB promoters DNA was essential for their constitutive processing. In support to this model, Liao and Sun demonstrated that the constitutive processing of p100ΔC mutants is regulated by their nuclear shuttling and abolished by mutation of their NLS (Liao and Sun, 2003). However, in our case, mutation of this NLS sequence did not prevent Hut78 to be constitutively processed into p52 as we could not observe any difference in the processing of our cytoplasmic mutant NLS1234 compared to the wild-type Hut78 (**Figure 20**). Moreover, mutation of the lysine 75, which is involved in the DNA-binding of p100, did not affect neither the processing of the protein Hut78.

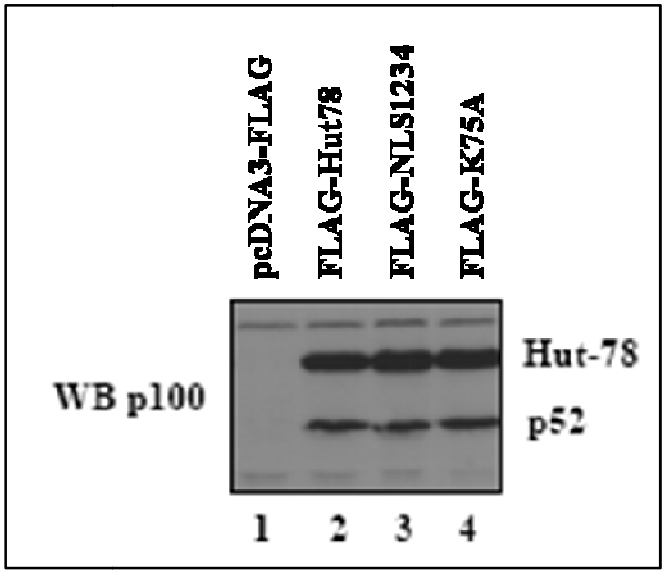

Figure 20: Hut78 as well as its mutants NLS1234 and K75A are constitutively processed into p52. HEK293 cells were transfected with the indicated expression plasmids and an anti-p100 Western blot was carried out on the cell extracts.

Hut78 interacts with multiple NF-κB/IκB proteins, coactivators and corepressors

Based on the nuclear staining of Hut78, we selected several proteins which are all known to be localized in the nucleus in order to identify Hut78-interacting proteins.

❖ *NF-κB/IκB proteins*

By immunoprecipitation assay in HUT78 cells, we first showed that p52, as well as the unprocessed Hut78, both interact with the NF-κB members p50, p65 (RelA) and RelB (**Figure 21**).We also showed an interaction between Hut78 and the nuclear IκB family member BCL-3, when we overexpressed both proteins in HEK293 cells (**Figure 22**).

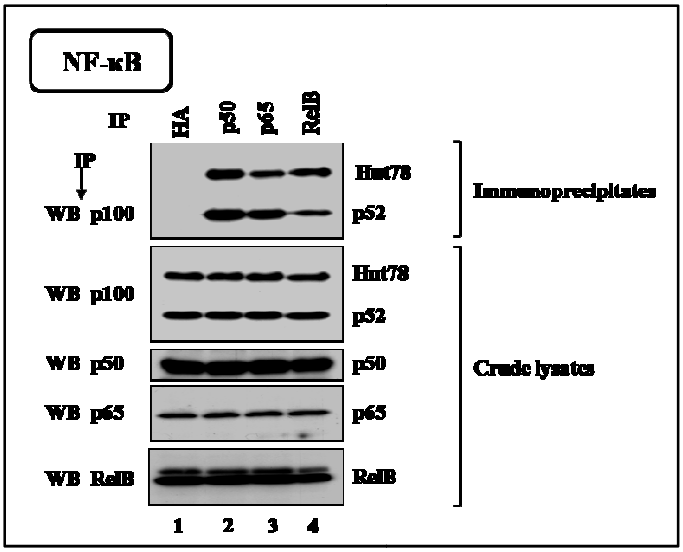

Figure 21: Hut78 and p52 bind to multiple NF-κB proteins. Cell extracts from HUT78 cells were subjected to anti-HA (negative control), -p50, -p65 or -RelB immunoprecipitations followed by anti-p100 western analysis (top panel, lanes 1 to 4, respectively). Cell extracts were also subjected to anti-p100, -p50, -p65 or -RelB analysis as well (bottom panels).

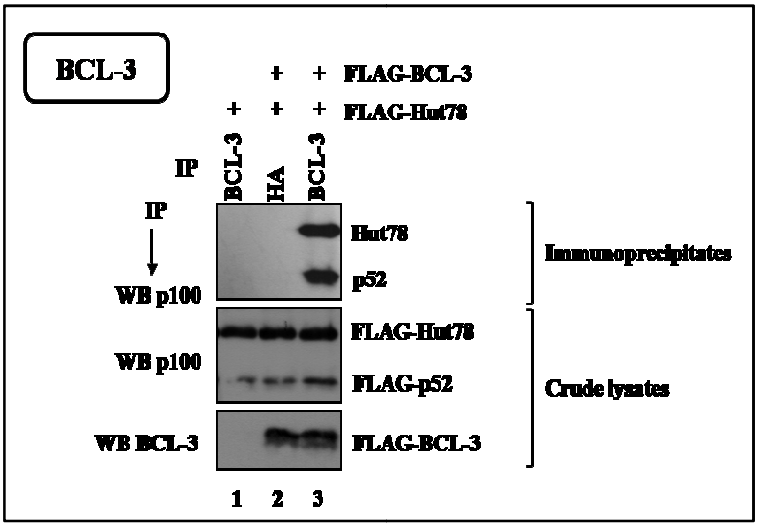

Figure 22: Hut78 binds BCL-3. HEK293 cells were transfected with the indicated expression plasmids and anti-HA (negative control) or -BCL-3 immunoprecipitations followed by anti-p100 western analysis were carried out on the cell extracts as indicated (top panel). The presence of Hut78 and BCL-3 in the cells extracts is illustrated by Western blot using the corresponding antibodies (bottom panels).

❖ ***HDACs***

Regulation of NF-κB-dependent gene expression requires the function of coregulatory proteins (coactivators or corepressors). Among these, some HDACs, which are generally found in large repressor complexes, bind directly or indirectly with NF-κB (p65/p50) to suppress basal gene expression (Ashburner *et al*., 2001; Bhat *et al*., 2008; Zhang and Kone, 2002). Interestingly, besides the vorinostat (Zolinza®), the romidepsin (also known as depsipeptide, FR901228, FK228), another histone deacetylase inhibitor isolated from the bacterium *Chromobacterium violaceum*, has also been reported to be effective in cutaneous T-cell lymphoma and is currently in clinical trials for this indication (Sandor *et al*., 2002; Piekarz *et al*., 2001). Romidepsin was shown to efficiently reduce both NF-κB and AP-1 DNA binding activity in HTLV-1 infected cell lines and in primary adult T-cell leukemia (ATL) cells (Mori *et al*. 2004). Moreover, treatment of HUT78 cells with romidepsin, as well as with other structurally distinct histone deacetylase inhibitors, including sodium butyrate, TSA (trichostratin A) or MS-275, caused increased histone acetylation, induction p21 expression, and marked apoptosis without significant cell cycle arrest (Piekarz *et al*., 2004). Taken together, these findings suggest a role of HDACs in the pathogenesis of T-cell lymphomas, particularly in Hut78-mediated cutaneous T-cell lymphomas. This led us to determine by co-immunoprecipitations, which HDACs associate with the Hut78 protein (**Figures 23, 24, 25** and **26**).

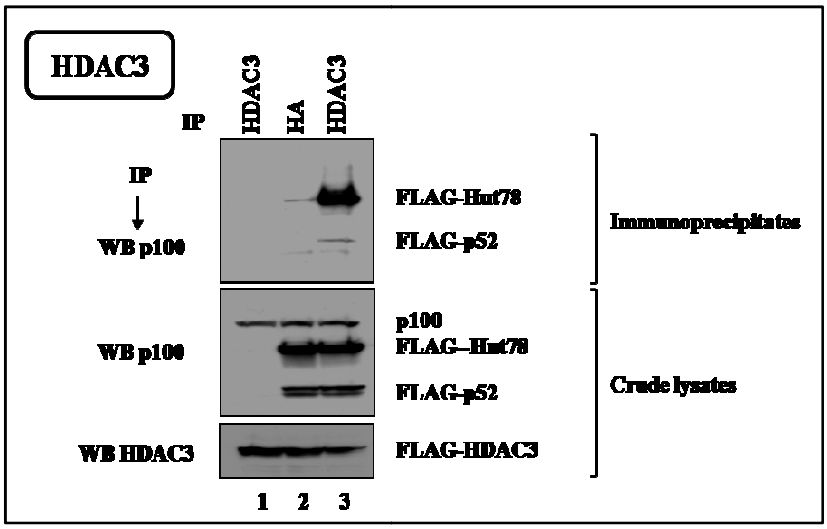

Figure 23: Hut78 interacts with HDAC3. HEK293 cells were transfected with a FLAG-HDAC3 vector, simultaneously with a FLAG-Hut78 (lanes 2, 3) or an empty vector (lane 1). Cell extracts were subjected to an anti-HA (lane 2) or -HDAC3 (lanes 1, 3) immunoprecipitations, followed by western analysis using the anti-p100 antibody (top panel). Crude cell extracts were also subjected to anti-p100 and -HDAC3 western analysis (middle and bottom panels).

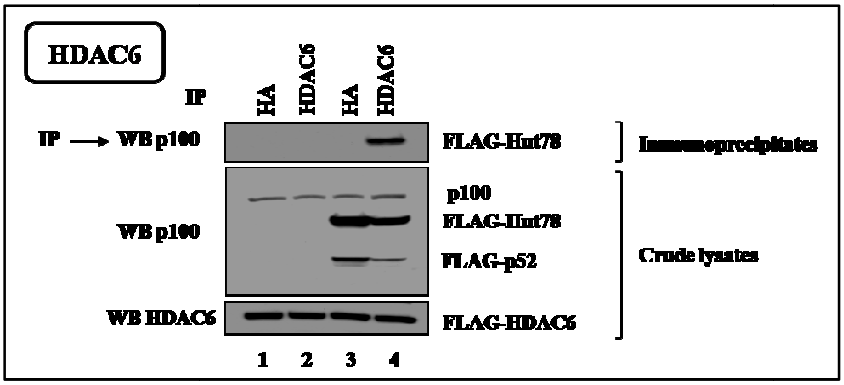

Figure 24: Hut78 interacts with HDAC6. HEK293 cells were transfected with a FLAG-HDAC6 vector, simultaneously with a FLAG-Hut78 (lanes 3, 4) or an empty vector (lanes 1, 2). Cell extracts were subjected to an anti-HA (lanes 1, 3) or -HDAC6 (lanes 2, 4) immunoprecipitations, followed by western analysis using the anti-p100 antibody (top panel). Crude cell extracts were also subjected to anti-p100 and -HDAC6 western analysis (middle and bottom panels).

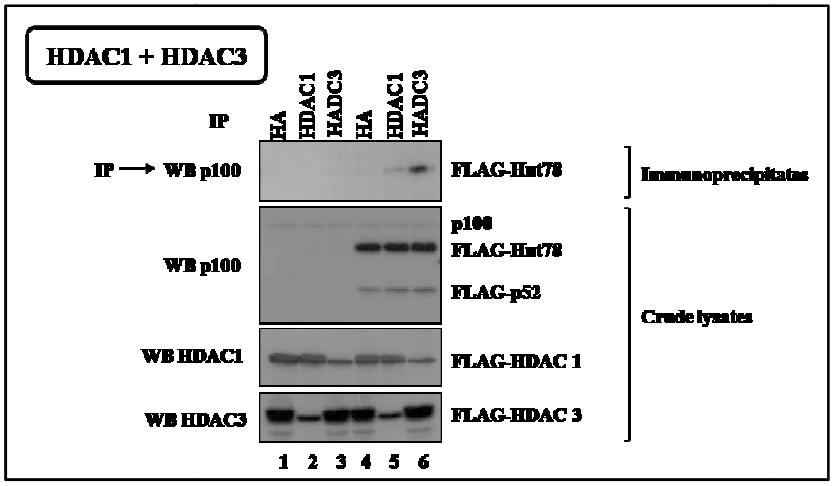

Figure 25: Hut78 weakly interacts with HDAC1, as compared with HDAC3. HEK293 cells were transfected with a FLAG-HDAC1 (lanes 1, 2, 4, 5) or FLAG-HDAC3 (lanes 1, 3, 4, 6) vector, simultaneously with a FLAG-Hut78 (lanes 4, 5, 6) or an empty vector (lanes 1, 2, 3). Cell extracts were subjected to an anti-HA (lanes 1, 4), -HDAC1 (lanes 2, 5) or -HDAC3 (lanes 3, 6) immunoprecipitations, followed by western analysis using the anti-p100 antibody (top panel). Crude cell extracts were also subjected to anti-p100, HDAC1 and -HDAC3 western analysis (bottom panels).

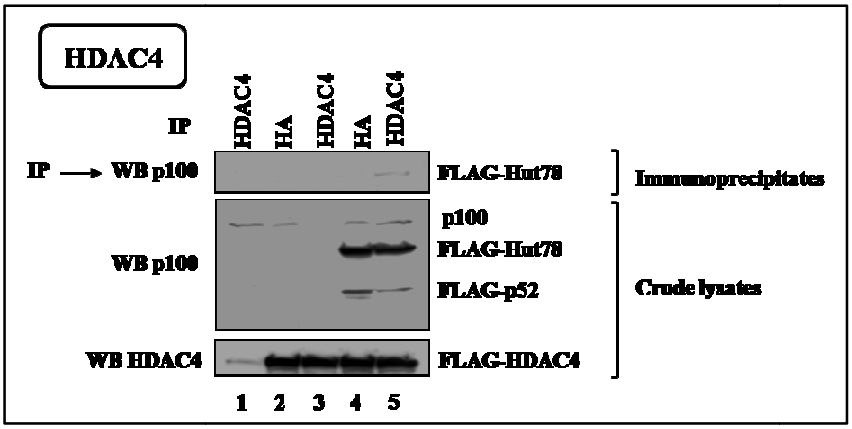

Figure 26: Hut78 doesn't interact with HDAC4. HEK293 cells were transfected with a FLAG-HDAC4 vector (lanes 2 to 5) or an empty vector (lane 1), simultaneously with a FLAG-Hut78 (lanes 4, 5) or an empty vector (lanes 1 to 3). Cell extracts were subjected to an anti-HA (lanes 2, 4) or -HDAC4 (lanes 1, 3, 5) immunoprecipitations, followed by western analysis using the anti-p100 antibody (top panel). Crude cell extracts were also subjected to anti-p100 and -HDAC4 western analysis (middle and bottom panels).

These results show that Hut78 interacts with HDAC3 and HDAC6, while no or weak interaction could be detected between Hut78 and HDAC4 or HDAC1, as compared to HDAC3. HDAC3 possesses both a nuclear import signal and a nuclear export signal, but is nearly always localized in the nucleus, in contrast to HDAC6, whose predominant localization is in the cytoplasm. However, HDAC6 is able to shuttle in and out of the nucleus in response to certain cellular signals and has been shown to interact with nuclear proteins like HDAC11 (Bertos *et al*., 2001; Gao *et al*., 2002).

Ashburner and colleagues showed that the region of p65 which interacts with HDAC1 lies within the Rel Homology domain (Ashburner *et al*., 2001), while Viatour and colleagues demonstrated the ankyrin repeats of IκBα are critical in mediating the interaction with HDAC3 (Viatour *et al*., 2003b). To identify the Hut78 domain(s) mediating the interaction with HDAC proteins, we next tested the ability of Hut78 mutants lacking different functional domains to interact with HDAC3.

Mutants lacking from one to five ankyrin repeats still bind HDAC3, suggesting that the C-terminal ankyrin repeats are dispensable for the interaction of Hut78 with HDAC3 (**Figure 27**). This result was not surprising as we observed that p52, which is devoid of ankyrin repeats, also associates with HDAC3. Therefore, the functional domain of Hut78 required for interaction with HDAC3 is located upstream the ankyrin repeats.

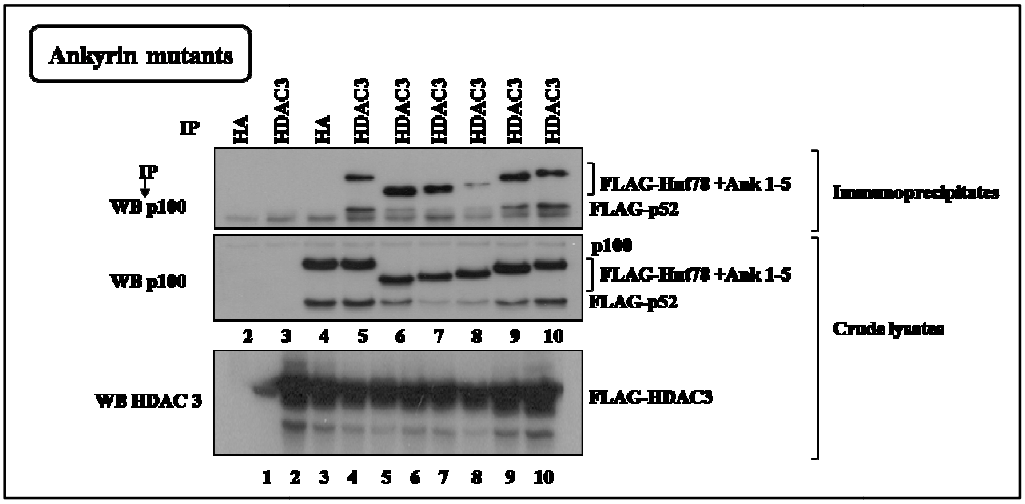

Figure 27: The C-terminal ankyrin repeats of Hut78 are dispensable for binding to HDAC3. HEK293 cells were transfected with a FLAG-HDAC3 vector (lanes 2 to 10) or an empty vector (lane 1), simultaneously with a FLAG-Hut78 (lanes 4, 5), FLAG-Ankyrin 1-5 (lanes 6 to 10, respectively) or an empty vector (lanes 1 to 3). Cell extracts were subjected to an anti-HA (lanes 2, 4) or -HDAC3 (lanes 3, 5 to 10) immunoprecipitations, followed by western analysis using the anti-p100 antibody (top panel). Crude cell extracts were also subjected to anti-p100 and -HDAC3 western analysis (middle and bottom panels).

We thus determined by co-immunoprecipitation if mutants lacking variable portions of the N-terminal Rel homology domain were still able to bind HDAC3 (**Figure 28**). Surprisingly, partial deletion of the RHD strongly enhanced the interaction with HDAC3. This stronger interaction with HDAC3 was also observed when we mutated the conserved lysine residue (K75), which is critical for DNA binding (Michalopoulos and Hay, 1999) (**Figure 29**). As expected, the p52 issued from the processing of this K75A mutant also exhibits enhanced binding affinity for HDAC3. Taken together, these results demonstrate that interaction between Hut78 and HDAC3 is negatively regulated by its DNA-binding domain.

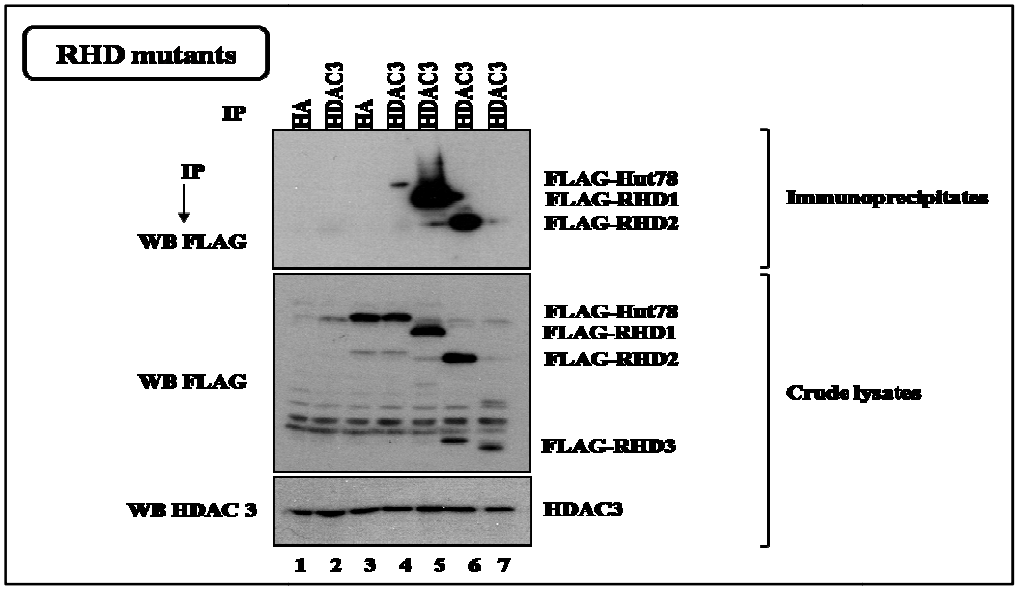

Figure 28: Hut78 mutants lacking variable portions of the RHD more strongly interact with HDAC3. HEK293 cells were transfected with a HDAC3 vector, simultaneously with a FLAG-HUT78 (lanes 3, 4), FLAG-RHD1-3 (lanes 5 to 7, respectively) or an empty vector (lanes 1, 2). Cell extracts were subjected to an anti-HA (lanes 1, 3) or -HDAC3 (lanes 2, 4 to 7) immunoprecipitations, followed by western analysis using the anti-FLAG antibody (top panel). Crude cell extracts were also subjected to anti-FLAG and -HDAC3 western analysis (bottom panels).

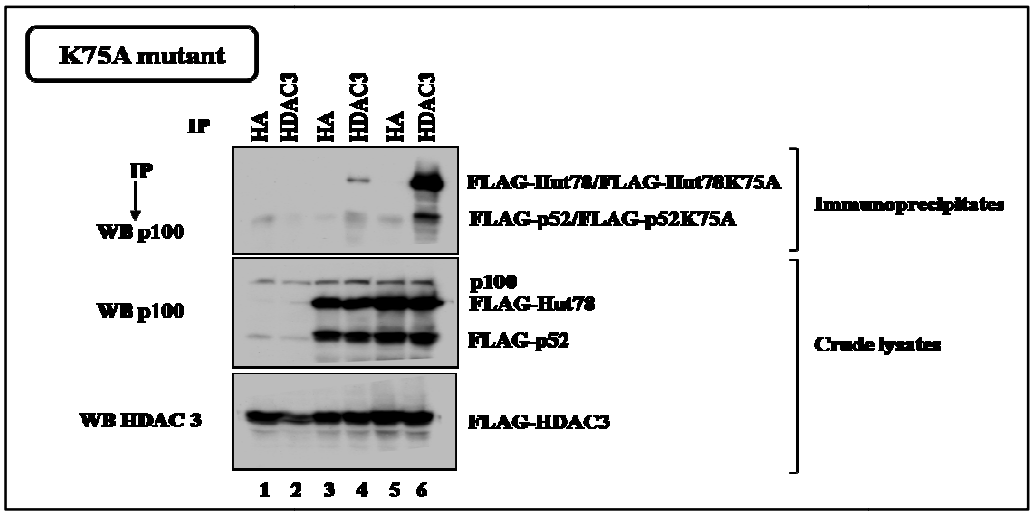

Figure 29: Hut78 mutant K75A more strongly interacts with HDAC3. HEK293 cells were transfected with a FLAG-HDAC3 vector, simultaneously with a FLAG-Hut78 (lanes 3, 4), FLAG-Hut78-K75A (lanes 5, 6) or an empty vector (lanes 1, 2). Cell extracts were subjected to an anti-HA (lanes 1, 3, 5) or -HDAC3 (lanes 2, 4, 6) immunoprecipitations, followed by western analysis using the anti-p100 antibody (top panel). Crude cell extracts were also subjected to anti-p100 and -HDAC3 western analysis (bottom panels).

Determination of the oncogenic potential of Hut78

Ciana and colleagues (Ciana *et al*., 1997) demonstrated the tumorigenic activity *in vivo* of Lyt-10Cα, another p100 C-terminally truncated mutant. They showed that constitutive expression of this protein in immortalized Balb/3T3 mouse fibroblasts did not affect the cells growth curves, but allows colony formation in soft agar and tumor development in immunodeficient mice, three weeks after injection. They were however unable to obtain clones expressing Hut78. To verify whether Hut78 was also capable of transforming mammalian cells *in vitro* and being tumorigenic *in vivo*, we cloned this protein in the pBabe retroviral vector and then infected immortalized NIH3T3 mouse fibroblasts. The clones expressing Hut78 were selected with puromycine. In the same manner, we also overexpressed in NIH3T3 cells the different Hut78 mutants we generated in order to evaluate the effects of diverse mutations/deletions on the oncogenic potential of Hut78 and further link them to functional properties, like subcellular localization, DNA binding, interaction with HDACs or absence of processing.

❖ ***Growth curves***

We first evaluated the proliferation of the NIH3T3 cells expressing p52, Hut78 or some of its mutant forms (NLS1234, ankyrin 1-5). The morphology and growth pattern of these cells were similar to cells infected by the control vector pBabe (**Figure 30**).

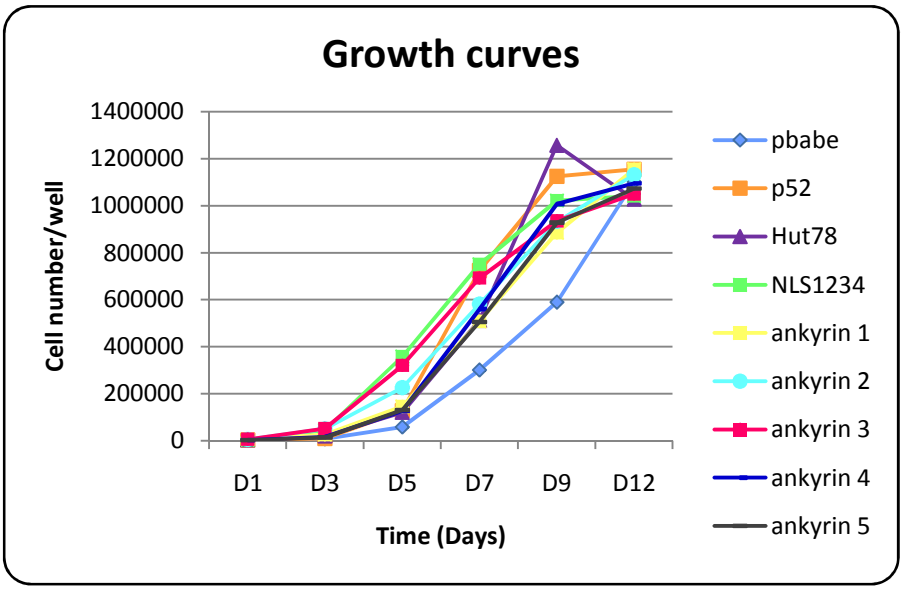

Figure 30: NIH3T3 cells over-expressing p52, Hut78 or its mutants NLS1234 and ankyrin 1-5 don't exhibit enhanced proliferative phenotype in comparison to control cells. Growth curves were established for NIH3T3 cells infected with the indicated retroviral construct by counting the number of cells every 2 days for 12 days.

❖ ***Foci formation assays***

We next assessed the oncogenicity of p52, Hut78 or its mutants *in vitro* by foci formation assays, but we could not observe any foci formation in the NIH3T3 cells expressing p52, Hut78 or its mutant forms, as compared to cells infected with an empty vector.

❖ ***Tumor development in immunodeficient mice***

To test the ability of Hut78 to form tumors *in vivo*, we injected the same NIH3T3 infected cells subcutaneously into nude mice and monitored the tumor development for 12 weeks. While mice injected with the positive control RasV12-expressing cells developed tumors within a few days, no tumor was detected in the mice injected with negative control cells or cells expressing p52, Hut78 or its different mutants during the period of experimentation.

Therefore, none of these experiments allowed us to demonstrate the oncogenic potential of Hut78 or its mutants *in vitro* or *in vivo*. This suggests that additional genetic or epigenetic alterations may be required for malignant transformation of Hut78 expressing cells. This idea is supported by the presence of other oncogenic rearrangements in the HUT78 cell line and the prolonged latency observed for the development of lymphomas in Hut78 transgenic mice (Thakur *et al*., 1994; Zhang *et al*., 2007).

Micro-arrays

We nevertheless decided to further explore the functional characteristics of Hut78 by identifying the genes specifically induced by this truncated NF-κB2 mutant. We thus performed micro-array analysis on NIH3T3 cells expressing p52 or Hut78, versus NIH3T3 cells infected by the empty vector pBabe. Surprisingly, only a few genes were upregulated on p52 or Hut78 overexpression in NIH3T3 and among those, *mmp9* was found to be the most strongly induced by both p52 and Hut78 (**Figure 31**). Interestingly, many human lymphoid tumor cells constitutively produce significant amount of MMP9 and elevated levels of MMP9 are associated with advanced stage and poor patient survival (Kossakowska *et al*., 1999; Vacca *et al*., 2000; Mori *et al*., 2002; Kamiguti *et al*., 2004; Sakata *et al*., 2004; Hazar *et al*., 2004). In patients with mycosis fungoides (MF) in particular, increased expression of MMP9 mRNA by tumor cells was reported to correlate with disease progression, from

patch (clustered lymphoid tumor T-cells within epidermis and superficial dermis) to nodular stage (clustered and scattered T-cells within epidermis and dermis in depth) (Vacca *et al.*, 2000). Therefore, these findings suggest that upregulation of MMP9 by Hut78 could account for the dissemination and deepening of MF cells in dermis and contribute to tumor invasion.

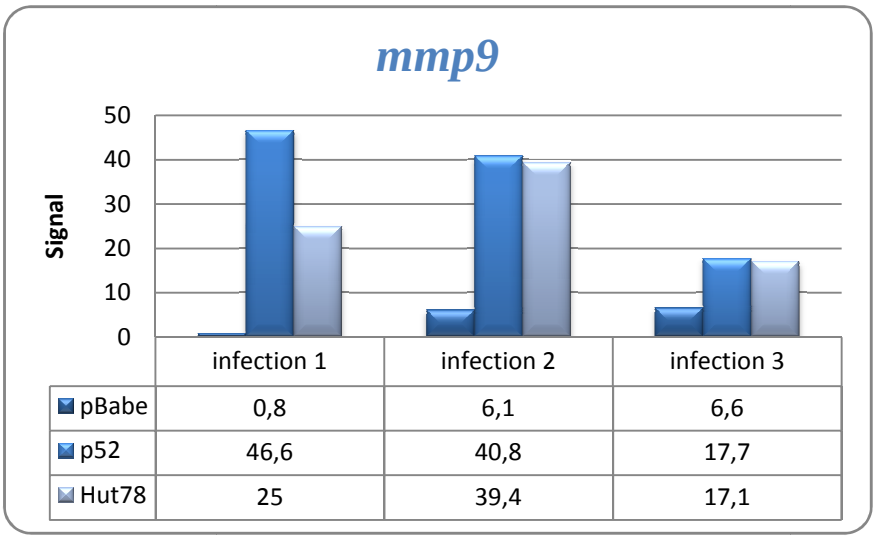

Signal Log-ratio	infection 1	infection 2	infection 3
p52 vs pBabe	5,4	2,8	1,1
Hut78 vs pBabe	4,1	3	0,9

Figure 31: Induction of *mmp9* gene expression on p52 or Hut78 overexpression in NIH3T3 cells. Total RNAs extracted from NIH3T3 cells infected with pBabe or with a p52 or Hut78 expressing retrovirus were subjected to micro-array analysis. The figure shows micro-array signal intensities from three distinct infections. The table below indicates the Signal Log-ratios, which measure the magnitude and direction of change between transcript levels of the experimental (p52 or Hut78) and control array (pBabe). Base 2 is used as the log scale, therefore a Signal Log-Ratio of 1 represents a two-fold increase in abundance of an mRNA.

Moreover, this micro-array analysis also revealed that the gene coding for the tissue inhibitor of matrix metalloproteinases 4 (TIMP-4) was down-regulated on p52 or Hut78 overexpression (**Figure 32**). Therefore, in addition to inducing *mmp9* gene expression, Hut78 negatively regulates one of its endogenous inhibitor, TIMP-4. The resulting imbalance between MMPs and TIMPs is thought to be a major determinant of the proteolytic potential of tumors (Folgueras *et al.*, 2004). Several studies showed that overproduction of TIMPs

inhibits experimental metastasis (DeClerck and Imren 1994), while low levels of TIMPS correlate with tumorigenesis (Khokha *et al.*, 1989; Cruz-Munoz *et al.*, 2006). TIMP-4 was shown to reduce tumorigenic and metastatic potentials of human breast cancer cells, presumably, in part, due to its anti-angiogenic activity (Wang *et al.*, 1997). However, TIMPs have also been associated with tumor progression, indicating that their role in cancer is also dual and complex (Baker *et al.*, 2002; Jiang *et al.*, 2002). High levels of TIMP-4 have been observed in endometrial and cervical carcinomas (Tunuguntla *et al.*, 2003; Lizarraga *et al.*, 2005) and in colorectal cancer, but in this latter case, it was related to longer survival of patients (Hilska *et al.*, 2007).

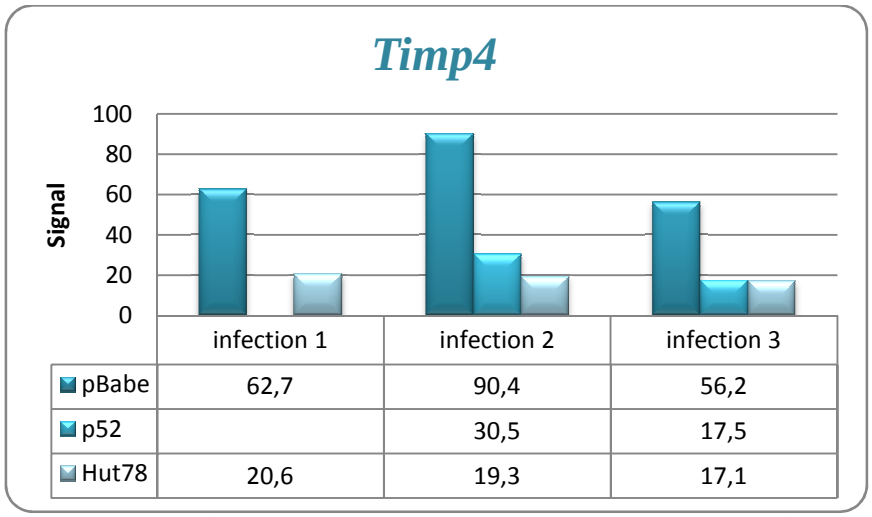

Signal Log ratio	infection 1	infection 2	infection 3
p52 vs pBabe		-1,6	-1
Hut78 vs pBabe	-1,7	-2,2	-1,4

Figure 32: *Timp-4* gene expression is decreased on p52 or Hut78 overexpression in NIH3T3 cells. Total RNAs extracted from NIH3T3 cells infected with pBabe or with a p52 or Hut78 expressing retrovirus were subjected to micro-array analysis. The figure shows micro-array signal intensities from three distinct infections. The table below indicates the Signal Log-ratios, which measure the magnitude and direction of change between transcript levels of the experimental (p52 or Hut78) and control array (pBabe). Base 2 is used as the log scale, therefore a Signal Log-Ratio of -1 represents a two-fold reduction in transcript expression.

The fact that we didn't find any gene involved in cellular growth or inhibition of apoptosis upregulated in NIH3T3 cells overexpressing p52 or Hut78, may explain why we couldn't observe any gain of proliferation of these cells in our experimental models.

Induction of *mmp9* gene expression by p52 and Hut78 in NIH3T3 cells

We next confirmed through Real-time PCR analysis the induction of *mmp9* gene expression in NIH3T3 cells overexpressing p52 or Hut78 (**Figure 33**). As control, we compared it to the IκBα mRNA levels which were increased by TNFα stimulation but not on p52 overexpression (**Figure 34**).

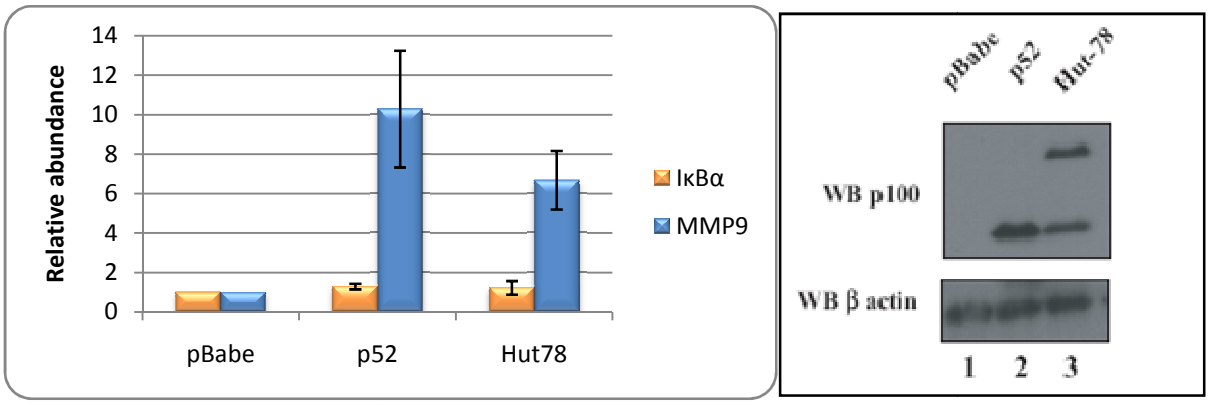

Figure 33: Induction of *mmp9* but not *IκBα* gene expression on p52 or Hut78 overexpression in NIH3T3 cells. Total RNAs from NIH3T3 cells infected with empty retroviral vector pBabe, the p52 or Hut78 expressing retrovirus were subjected to quantitative Real-Time PCR analysis to assess IκBα and MMP9 mRNA levels using the appropriate primers. The abundance of the IκBα or MMP9 mRNA levels in NIH3T3 cells infected with the empty pBabe was set to 1 and levels of both transcripts in p52 or Hut78 overexpressing NIH3T3 cells were relative to that after normalization with GAPDH. The figure shows the data from six independent experiments performed on two distinct infections (mean values ± S.D.). On the right panel, total cell extracts from those NIH3T3 cells infected with the empty retroviral vector pBabe or with a retroviral construct expressing p52 or Hut78 were subjected to anti p100 and β-actin Western blot analysis.

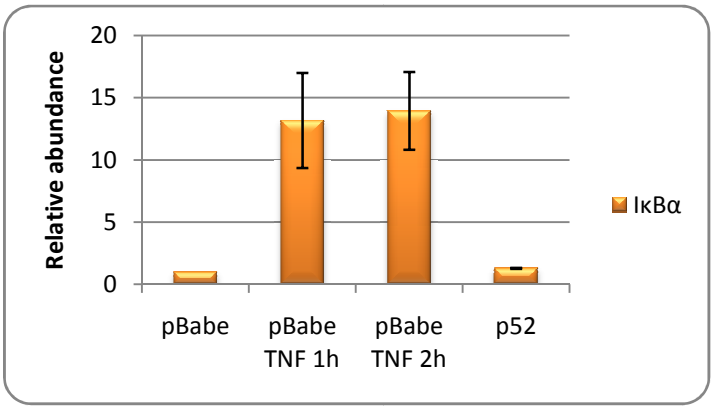

Figure 34: Induction of *IκBα* gene expression on TNFα stimulation, but not on p52 overexpression in NIH3T3 cells. NIH3T3 cells infected with pBabe or with the p52 expressing retrovirus were left untreated or stimulated with TNFα for the indicated periods of time and the abundance of the IκBα mRNA levels was assessed by Real-Time PCR analysis. IκBα mRNA levels in untreated NIH3T3 cells infected with pBabe were set to 1 and levels of this transcript in the other experimental conditions were relative to that after normalization with GAPDH. The figure shows the data from 2 independent experiments performed in duplicates (mean values ± S.D.).

We also examined MMP9 activity released from these NIH3T3 cells using gelatin zymography assays (**Figure 35**). We observed that MMP9 was secreted into serum-free medium by NIH3T3 cells overexpressing p52 or Hut78, but not or faintly by control cells. These results suggest that p52 and Hut78 overexpressing NIH3T3 not only have a higher level of *mmp9* gene expression but that they also release biologically active MMP9 protein into medium.

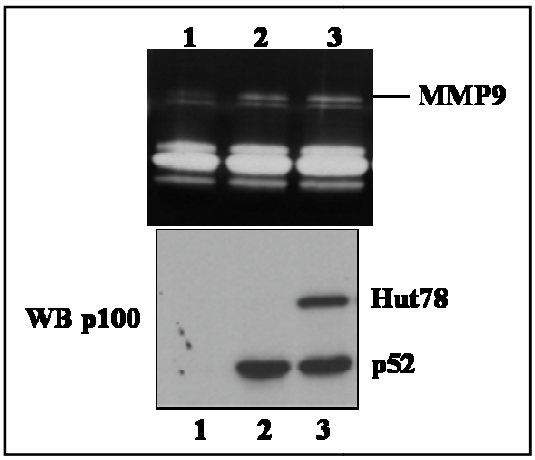

Figure 35: Hut78 or p52 overexpression in NIH3T3 cells enhances their gelatinase activity. Gelatinase activity in 48h conditioned medium from NIH3T3 cells infected with empty pBabe (**1**), pBabe p52 (**2**) or pBabe Hut78 (**3**) (upper panel). An anti-p100 Western blot was performed using cell extracts from these NIH3T3 cells (bottom panel).

Induction of *mmp9* gene expression on Hut78 overexpression in lymphoma cells

We next wanted to determine whether Hut78 over-expression also triggered *mmp9* gene induction in lymphoma-derived cells. We therefore compared the MMP9 mRNA levels in the mouse thymic lymphoma cell line 164T2 stably transfected with Hut78 pcDNA3-FLAG or with an empty vector. As indicated by the Western blots, p52 and Hut78 were well expressed in the Hut78-transfected cells, while RelB and p50 levels remained similar to the ones detected in control cells. There again, RT-PCR analysis showed an induction of *mmp9*, but not *IκBα* gene expression in the Hut78-overexpressing 164T2 cells (**Figure 36**).

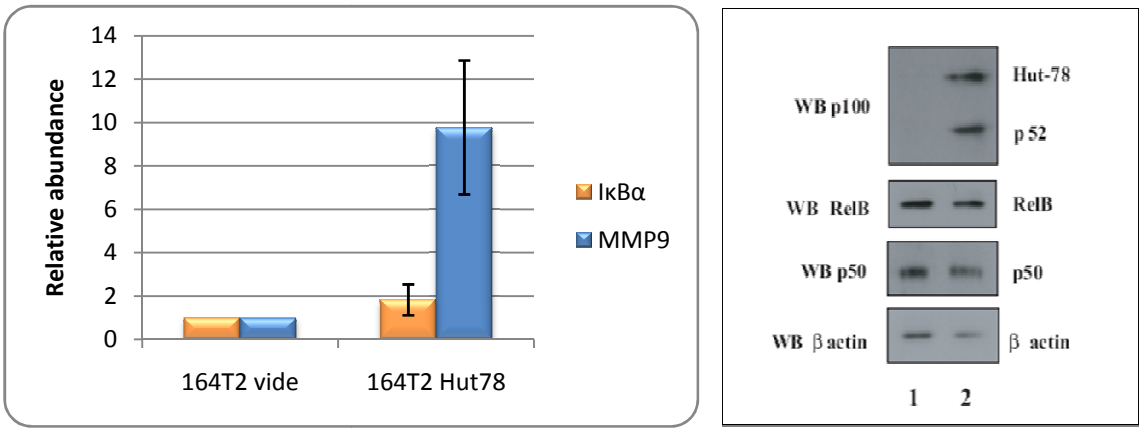

<u>Figure 36</u>: Hut78 overexpression in lymphoma cells triggers *mmp9*, but not *IκBα* gene expression. Total RNAs from 164T2 cells stably transfected with an empty vector or with a FLAG-tagged Hut78 expression plasmid were subjected to Real-Time PCR analysis to assess MMP9 and IκBα mRNA levels. The abundance of the IκBα or MMP9 mRNA levels in 164T2 cells transfected with the empty vector was set to 1 and levels of both transcripts in Hut78-overexpressing 164T2 cells were relative to that after normalization with GAPDH. The figure shows the data from two independent experiments performed in duplicates (mean values ± S.D.). On the right panel, cell extracts from those 164T2 cells stably transfected with an empty vector (**1**) or with a FLAG-tagged Hut78 expression plasmid (**2**) were subjected to Western blot analysis using the anti-p100, -RelB, p50 or β-actin antibodies, as indicated.

In order to determine if overexpression of Hut78 and thus MMP9 confers a more aggressive phenotype to 164T2 cells, we injected in the caudal vein of nude mice, 164T2 cells stably transfected with an empty vector or with a Hut78 expression plasmid and compared the development of tumors and metastases. As a positive control, we injected 164T2 S19 cells, highly metastatic clones derived from the 164T2 cell which produce constitutively high levels of MMP9. While mice injected with 164T2 S19 cells developed tumors within a few weeks, no tumor formation was observed in mice injected with 164T2 cells, expressing Hut78 or not, during the time of experimentation (3 months). Moreover, we kept some 164T2 cells overexpressing Hut78 in culture, with G418 selection, and regularly checked the expression of Hut78. After several weeks, we observed a severe decrease in the Hut78 protein level. Therefore, the expression of Hut78 in 164T2 injected in mice also probably disappeared after a time and, due to the late onset of tumor formation, we were not able to maintain a stable Hut78 expression level for the period necessary to observe tumors and metastases development.

Decreased MMP9 levels on p52 depletion in HUT78 cells

The next logical complementary approach to demonstrate that *mmp9* was a p52/Hut78-dependent target gene was to deplete p52 in the HUT78 cell line and to observe the effect on the expression of MMP9. For this purpose, we used a shRNA lentiviral construct that specifically targets p100/p52. MMP9 mRNA levels were decreased in those p52-depleted HUT78 cells as compared to cells infected with a control shRNA lentiviral construct (**Figure 37**).

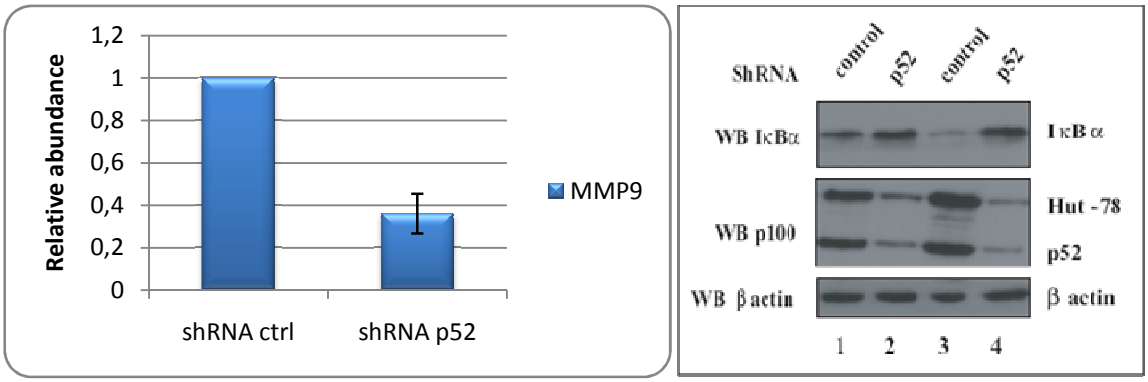

Figure 37: Decreased MMP9 mRNA levels on p52 depletion in HUT78 cells. On the right panel, HUT78 cells were infected with a lentiviral shRNA control (lanes 1, 3) or targeting p52 (lanes 2, 4) and cell extracts from these infected cells were subjected to anti-IκBα, -p100 and -β-actin Western blot analysis. On the left panel, MMP9 mRNA levels using total RNA from HUT78 cells infected with the control or with the shRNA p52 lentiviral constructs were quantified by Real-Time PCR analysis. MMP9 mRNA level in HUT78 cells infected with the control shRNA was set to 1 and levels of this transcript in the other experimental condition were relative to that after normalization with 18S. The figure shows the data from five independent experiments performed in duplicates (mean values ± S.D.).

Interestingly, we also observed that IκBα accumulates at the protein level in p52-depleted HUT78 cells, which indicates that p52 may be required to repress IκBα expression in these cells (**Figure 37**).

Zymography analysis indicated that HUT78 cells constitutively secreted MMP9 into the supernatant and that this secretion was impaired in p52/Hut78-depleted cells (**Figure 38**). This deficiency was specific to MMP9 as the secretion of MMP2 was not significantly altered by p52/Hut78 depletion. In agreement with our results in NIH3T3 cells, we can conclude that *mmp9* is a p52/Hut78-dependent target gene as both MMP9 enzymatic activity and mRNA expression correlated with the p52/Hut78 protein levels.

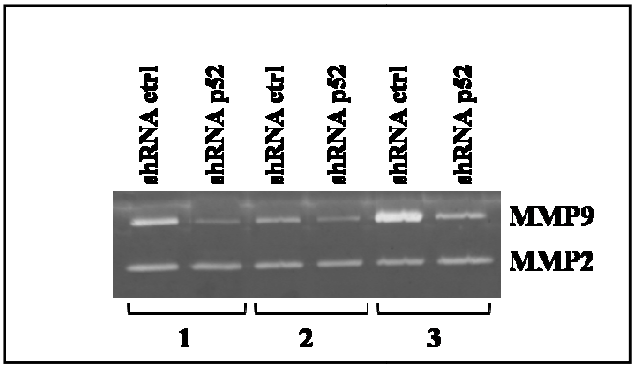

Figure 38: Impaired gelatinase activity in p52-depleted HUT78 cells. Conditioned media from HUT78 cells infected with the control shRNA or with the shRNA p52 were subjected to zymography analysis. The upper band corresponds to MMP9 and the lower to MMP2. This experiment was performed on three independent infections (**1**, **2**, **3**).

Invasion assay

To evaluate the role of MMP9 induction by p52/Hut78 on the invasive phenotype of HUT78 cells, we measured the migration of HUT78 cells depleted or not with p52/Hut78, across a basement membrane matrix preparation (Matrigel). We observed that p52/Hut78 depletion in HUT78 cells reduced their migration ability in Matrigel-coated transwells, suggesting that the p52/Hut78-induced MMP9 expression is required for the invasive potential of HUT78 cells (**Figure 39**).

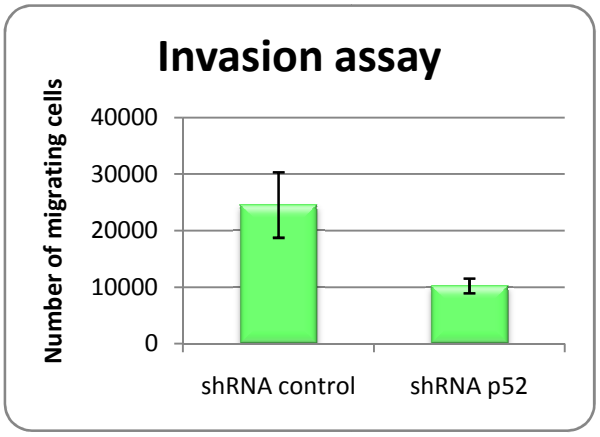

Figure 39: Impaired invasive potential in p52-depleted HUT78 cells. HUT78 cells infected with the indicated shRNA constructs were subjected to Matrigel invasion assay and the number of migrating cells was plotted. The figure shows the representative results (mean values ± S.D.) from two independent infections.

This *in vitro* migration assay was shown to reflect the invasive behavior of tumor cells *in vivo* (Shaw, from Jun-Lin Guan, Methods in Molecular Biology Cell Migration Developmental Methods and Protocols Vol 294, p97). In order to investigate this latter, we wanted to confirm these results *in vivo* by comparing the tumor formation in mice injected with HUT78 cells depleted or not with p52. However, development of tumor in HUT78 injected mice is a very slow process and we failed to maintain a stable p52 depletion during all the time needed for this experimentation.

Induction of *mmp9* gene expression by p52-producing NF-κB2 truncated mutants

We also found interesting to explore the ability of other NF-κB2 truncated proteins to induce *mmp9* gene expression. The p100HB mutant, detected in several human tumor cell lines (Derudder *et al*., 2003), originates from a point mutation generating a premature stop-codon and retains the entire ankyrin-repeats domain, but lacks the major part of the processing inhibitory domain (PID) (**Figure 40**). In the case of the LB40 p100ΔC mutant, which was cloned from a case of B-CLL (Migliazza *et al*., 1994), the NF-κB2 reading frame was found to be interrupted by a stop codon within the sixth ankyrin repeat. Like Hut78, these mutants are both located in the nucleus, but while LB40 constitutively generates p52, p100HB is mainly unprocessed.

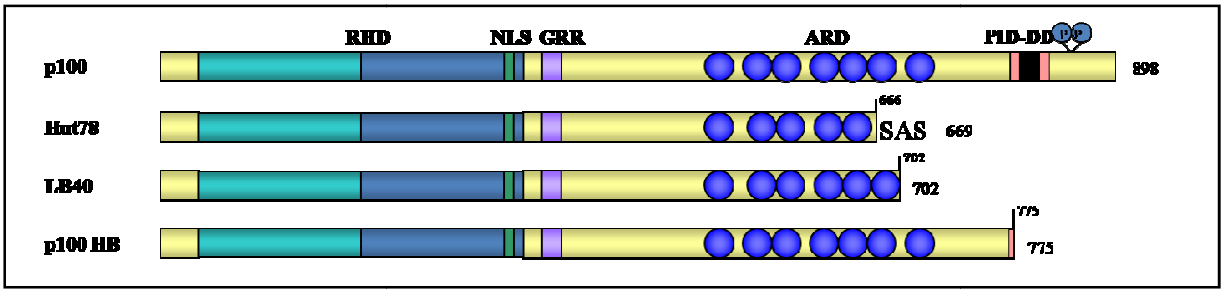

Figure 40: Schematic representation of p100 and different C-terminally NF-κB2 truncated mutants: Hut78, LB40 and p100HB. RHD: Rel homology domain, **NLS**: nuclear localization signal, **GRR**: glycine-rich region, **ARD**: ankyrin-repeats domain, **PID**: processing inhibitory domain, **DD**: death domain. The number of amino acids of each protein is indicated on the right. The number of amino acids derived from the normal NF-κB2 sequence is also shown for each protein.

We cloned the genes encoding these two proteins into the retroviral vector pBabe and infected NIH3T3 cells with these constructs. We observed that MMP9 was also strongly induced in NIH3T3 cells overexpressing the p52-producing LB40 protein, while p100HB, which barely generates p52, did not induce MMP9 in those cells (**Figure 41**).

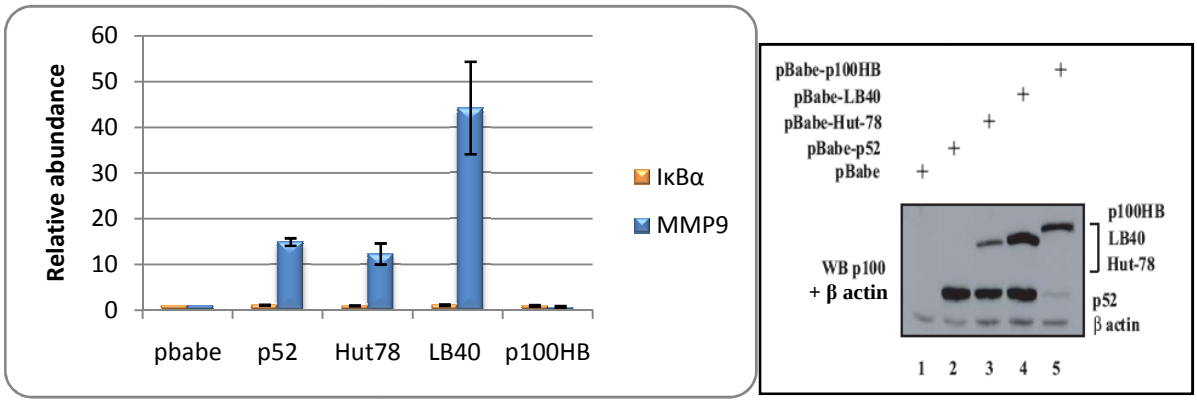

Figure 41: Overexpression of both Hut78 and LB40, but not p100HB triggers *mmp9* gene expression. Total RNAs from NIHT3T3 cells infected with the indicated retrovirus were subjected to Real-Time PCR analysis to assess IκBα and MMP9 mRNA levels. The abundance of IκBα or MMP9 mRNA levels in NIH3T3 cells infected with the empty pBabe was set to 1 and levels of both transcripts in other experimental conditions were relative to that after normalization with GAPDH. The figure shows the data from three independent experiments performed in duplicates (mean values ± S.D.). On the right panel, total cell extracts from those NIH3T3 cells infected with the indicated retrovirus were subjected to anti p100 and β-actin Western blot analysis.

Therefore, these results strongly suggest that *mmp9* gene induction by the truncated NF-κB2 proteins requires their constitutive processing into p52. To further investigate this issue, we decided to generate a processing-deficiency Hut78-mutant and to test its ability to induce *mmp9* gene expression.

Role of the GRR in p52/Hut78-induced *mmp9* gene expression

Xiao and colleagues identified the amino acid D415 of p100 as a proteasomal cleavage site required for the constitutive processing of LB40 and other p100ΔC mutants (Qing *et al.*, 2007). However, substitution of this single amino acid with alanine in the Hut78 sequence was not sufficient to prevent its constitutive processing. Therefore, in order to determine the contribution of the constitutive enhanced production of p52 in Hut78-induced *mmp9* gene expression, we generated a mutant which was no more processed in p52 by deleting the glycine-rich region (GRR) (Heusch *et al.*, 1999) (**Figure 42**). We observed that *mmp9* was weakly induced in NIH3T3 cells overexpressing the processing-deficient mutant Hut78ΔGRR, as compared to cells expressing p52 or Hut78 (**Figure 43**). Nevertheless, deletion of the glycine-rich region in p52 also dramatically decreased its ability to induce *mmp9* gene expression.

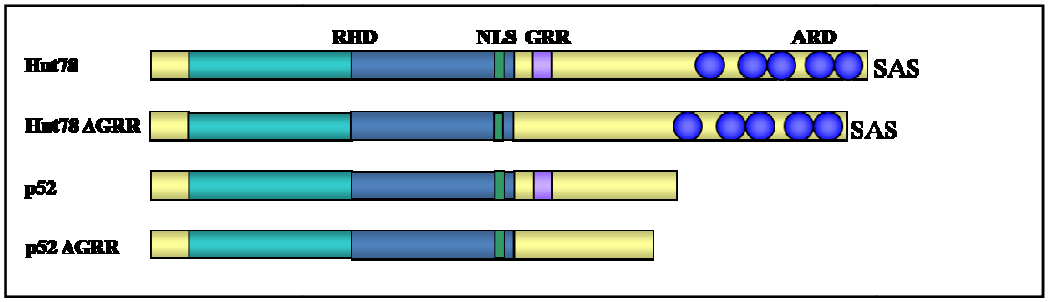

Figure 42: Schematic representation of p52, Hut78 and their ΔGRR mutants. RHD: Rel homology domain, **NLS**: nuclear localization signal, **GRR**: glycine-rich region, **ARD**: ankyrin-repeats domain.

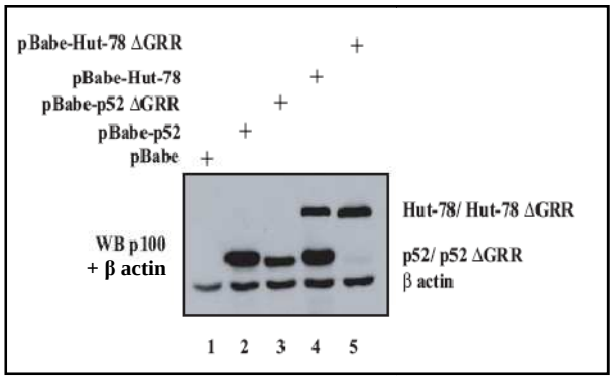

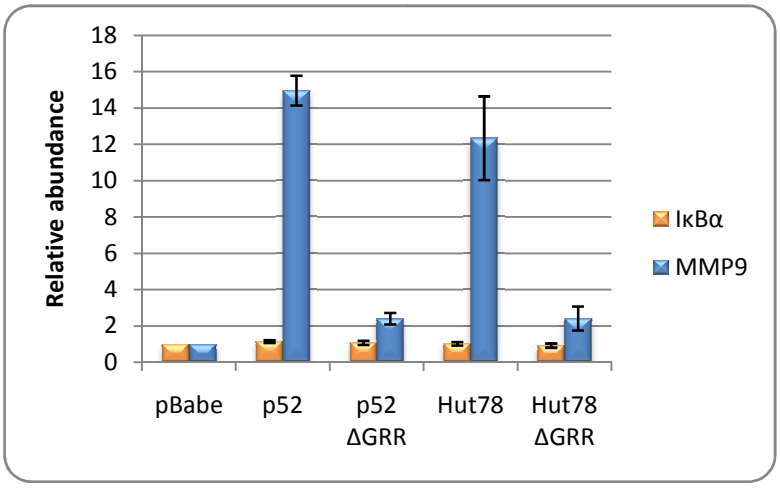

Figure 43: *mmp9* gene induction in NIH3T3 requires a functional GRR domain. Top panel: total cell extracts from NIH3T3 cells infected with the indicated retrovirus were subjected to anti p100 and β-actin Western blot analysis. Bottom panel: total RNAs from NIHT3T3 cells infected with the indicated retrovirus were subjected to RT PCR analysis to assess IκBα and MMP9 mRNA levels. The abundance of the IκBα or MMP9 mRNA levels in NIH3T3 cells infected with the empty pBabe was set to 1 and levels of both transcripts in other experimental conditions were relative to that after normalization with GAPDH. The figure shows the data from three independent experiments performed in duplicates (mean values ± S.D.).

Therefore, we cannot conclude from this experiment that Hut78-induced *mmp9* transcriptional activation occurs through p52 overproduction as the GRR domain seems to be required for *mmp9* gene induction. However, the p100HB mutant, which is nuclear like Hut78, but barely processes into p52, still harbors the GRR domain, but fails to induce *mmp9* expression in NIH3T3 cells. Therefore, our data collectively suggest that MMP9 transcriptional induction requires a functional GRR domain and support the model in which the processed p52 contributes to the oncogenicity of p100ΔCs by inducing a subset of tumor-associated genes.

Role of the alternative pathway in *mmp9* gene expression regulation

If *mmp9* has been demonstrated to be a target gene of the classical NF-κB-activating pathway (Bond *et al*., 1998; Bond *et al*., 2001), the contribution of the alternative pathway in its regulation has not been really investigated so far. However, in a recent study, increased levels of MMP9 were observed in the mammary glands of transgenic mice where p100/p52 was up-regulated during pregnancy and lactation (Connelly *et al*., 2007). These results are consistent with our findings, showing an induction of MMP9 in mouse fibroblasts overexpressing p52, and together, they suggest a role for the alternative pathway in the regulation of expression of MMP9.

To address this issue, we decided to compare the induction of MMP9 in MEF cells in which the classical NF-κB activating pathway was abolished or not. We stimulated these cells with either TNFα, a pro-inflammatory cytokine that does not directly activate the alternative pathway, or either with the LTβR agonistic antibody, which is known to trigger both the classical and the alternative pathways (Dejardin *et al*., 2002):

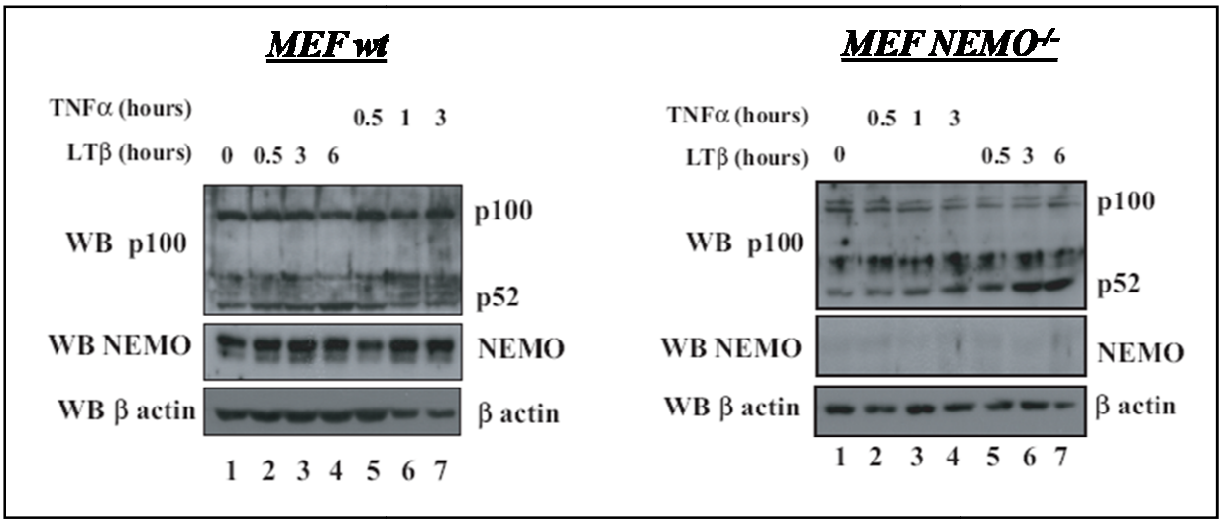

Figure 44: Unaltered LTβ mediated p100 processing into p52 in NEMO deficient MEF cells. MEFs wild type and NEMO deficient were left untreated (lanes 1) or stimulated with the indicated periods of time with an LTβR agonistic antibody or with TNFα and cell extracts from those cells were subjected to anti-p100, -NEMO and β-actin Western blot analysis, as indicated.

♦ As expected, TNFα had no effect on p100 processing neither in wild type MEFs, neither in NEMO deficient MEFs (**Figure 44**, lanes 5 to 7 compared to lane 1 for MEF wt and lanes 2 to 4 compared to lane 1 for MEF NEMO$^{-/-}$). In

contrast, the LTβR agonistic antibody induced p100 processing into p52 in both wild type MEFs and NEMO deficient MEFs, as seen by the increasing amount of p52 on LTβ stimulation (**Figure 44,** lanes 2 to 4 compared with lane 1 for MEF wt and lanes 5 to 7 compared with lane 1 for MEF NEMO$^{-/-}$).

♦ IκBα and MMP9 mRNA levels were increased on TNFα stimulation in wild type MEFs, but not in NEMO deficient MEFs, confirming that the classical NF-κB-activating pathway is no more functional in those cells (**Figure 45**).

♦ Both IκBα and MMP9 were also induced in wild type MEFs on LTβ stimulation, but, in contrast to TNFα stimulation, these inductions were not impaired in NEMO-deficient MEFs (**Figure 45**).

These results suggest that the alternative pathway can contribute alone to the regulation of *mmp9* gene expression in MEF cells.

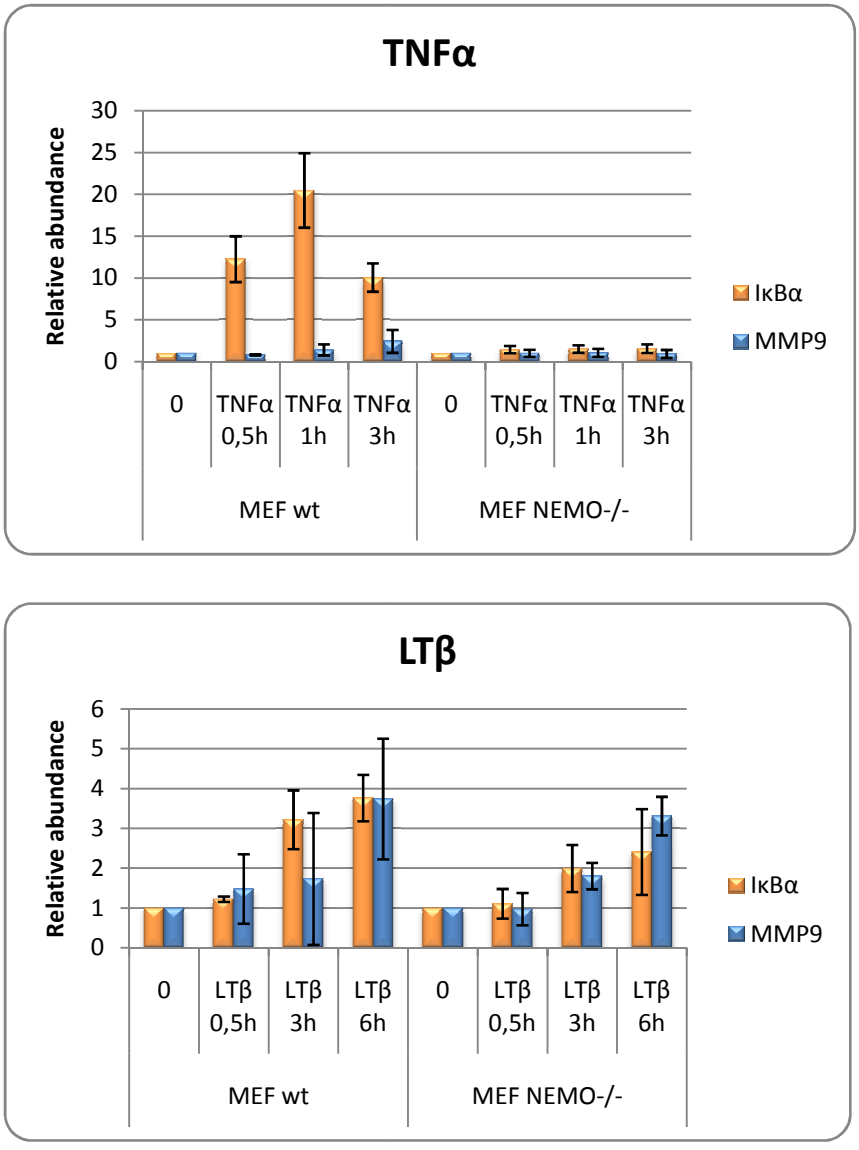

Figure 45: LTβ, but not TNFα mediates transcriptional induction of MMP9 and IκBα in NEMO deficient cells. Total RNAs from TNFα- (upper panel) or LTβ- (lower panel) stimulated wild type or NEMO deficient cells were subjected to quantitative RT-PCR analysis to assess IκBα and MMP9 mRNA levels. The abundance of the IκBα or MMP9 mRNA levels in unstimulated cells was set to 1 and levels of both transcripts in TNFα- or LTβ-stimulated cells were relative to that after normalization with GAPDH. The figure shows the data from three independent experiments (mean values ± S.D.).

Hut78 and p52-mediated MMP9 transcriptional induction involves the recruitment of a H3K4 HMT complex

As seen in the introduction, trimethylation of lysine 4 on histone H3 in the promoter region of genes has been linked to transcriptional activation. We thus decided to investigate the methylation status of the κB site of the *mmp9* and *IκBα* promoters (**Figure 47**) on p52 or Hut78 overexpression in NIH3T3 cells. ChIP assays performed with an antibody specifically targeting H3K4me3 indicated a robust H3K4 trimethylation on the *mmp9*, but not on the *IκBα* promoter in NIH3T3 cells overexpressing p52 or Hut78, as compared with control cells (**Figure 46**). Moreover, this methylation level correlates with the ability of proteins to induce *mmp9* gene expression as a much weaker H3K4 trimethylation was observed with a mutant (Hut78 ΔGRR) that failed to induce *mmp9* gene expression.

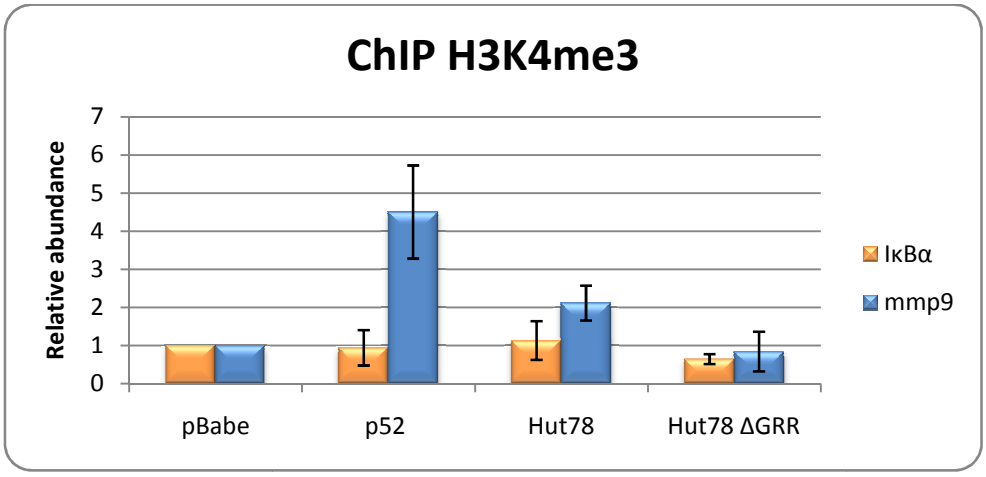

Figure 46: H3K4 trimethylation on the *mmp9* gene promoter on p52 or Hut78 overexpression in NIH3T3 cells. ChIP assays using an anti-H3K4me3 antibody were performed on DNA extracts from NIH3T3 cells infected with the empty pBabe or the retrovirus expressing p52, Hut78 or the Hut78ΔGRR mutant. Primers were derived from the promoter region of *mmp9* and *IκBα* genes and were designed to amplify a fragment that includes κB sites. The recruitment of the H3K4me3 activity in the NIH3T3 cells infected with the empty pBabe construct was set to 1 and its levels in the other conditions were relative to that after normalization with H3. The Figure shows the data from three independent experiments performed in duplicates (mean values ± S.D).

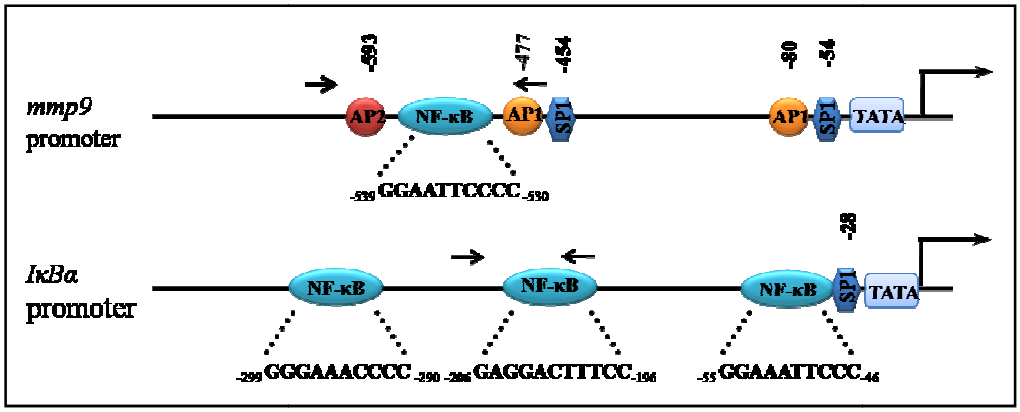

Figure 47: Schematic representation of the promoter sequences of both *mmp9* and *IκBα* murine genes. The NF-κB, AP1/2, Sp1 binding sites and the TATA box are illustrated. The arrows indicate the primers used in ChIP assays.

Conversely, the H3K4me3 activity was impaired on p52 depletion in HUT78 cells as shown on **figure 48**.

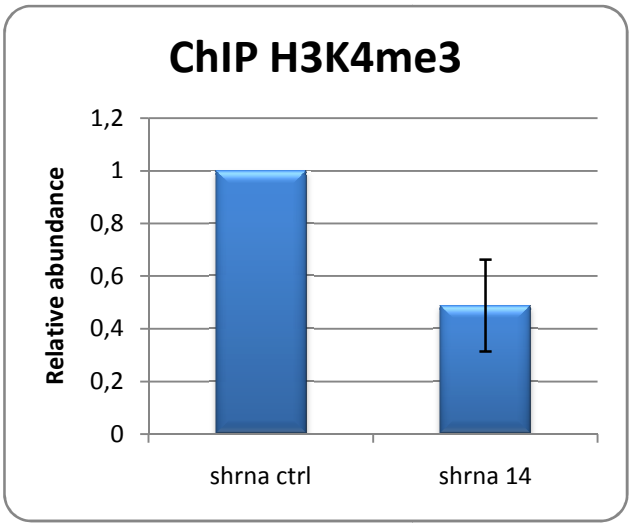

Figure 48: Impaired recruitment of the H3K4me3 activity in p52-depleted HUT78 cells. ChIP assays on HUT78 cells infected with the indicated shRNA constructs were carried out using an anti-H3K4me3 antibody. The signal obtained from a noncoding region (downstream of the albumin gene (Kouskouti and Talianidis, 2005)) was used to compensate for possible fluctuations arising during handling. The H3K4me3 ChIP values in HUT78 cells infected with the control shRNA construct was set to 1 and its value in the HUT78 cells infected with the shRNA p52 was relative to that after normalization with the total H3 signal (as detected using the corresponding anti-H3 antibody). The figure shows the data obtained from five independent experiments performed on two distinct infections (means ± S.D.).

These results suggest that p52 induces *mmp9* gene expression by specifically tethering a histone H3K4 methyltransferase complex. To more precisely define the relevance of this model, we next investigated by co-immunoprecipitation experiments, whether p52 could interact with the common subunits of these H3K4 HMT complexes, ASH2L, WDR5 and RbBP5. We found that p52 doesn't bind WDR5 nor RbBP5, but associates with ASH2L, although not as strongly as with BCL-3, used as a positive control (**Figure 49**).

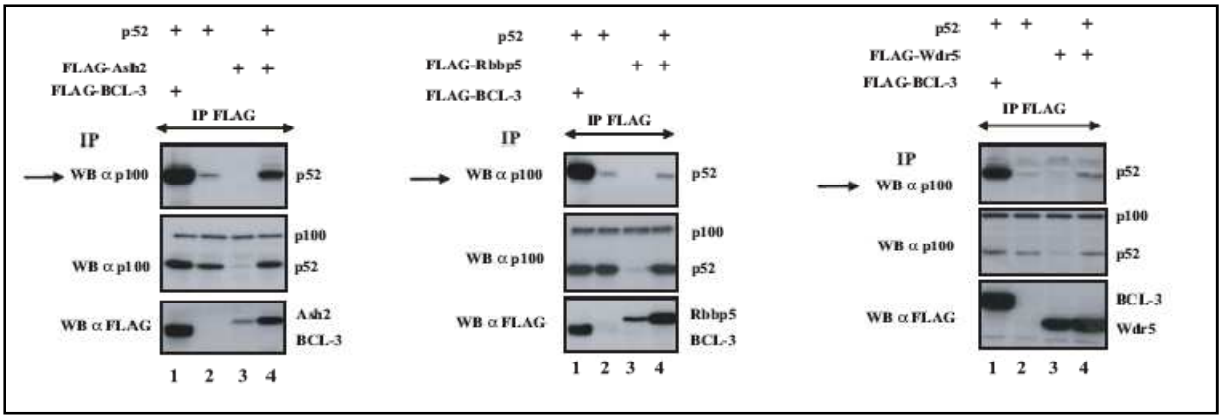

Figure 49: Association of p52 with ASH2L but not with RbBP5 and WDR5. HEK293 cells were transfected with the indicated expression plasmids and anti-FLAG immunoprecipitates followed by anti-p100 Western blot analysis were carried out on the cell extracts (top panels). Anti-p100 and -FLAG Western blots were performed on the crude cell extracts as well (bottom panels). (Performed with M. Aussems).

Moreover, we showed by immunofluorescence experiments that p52 and Hut78 colocalized with ASH2L in the nucleus, while the cytoplasmic mutant NLS1234 did not (**Figure 50**).

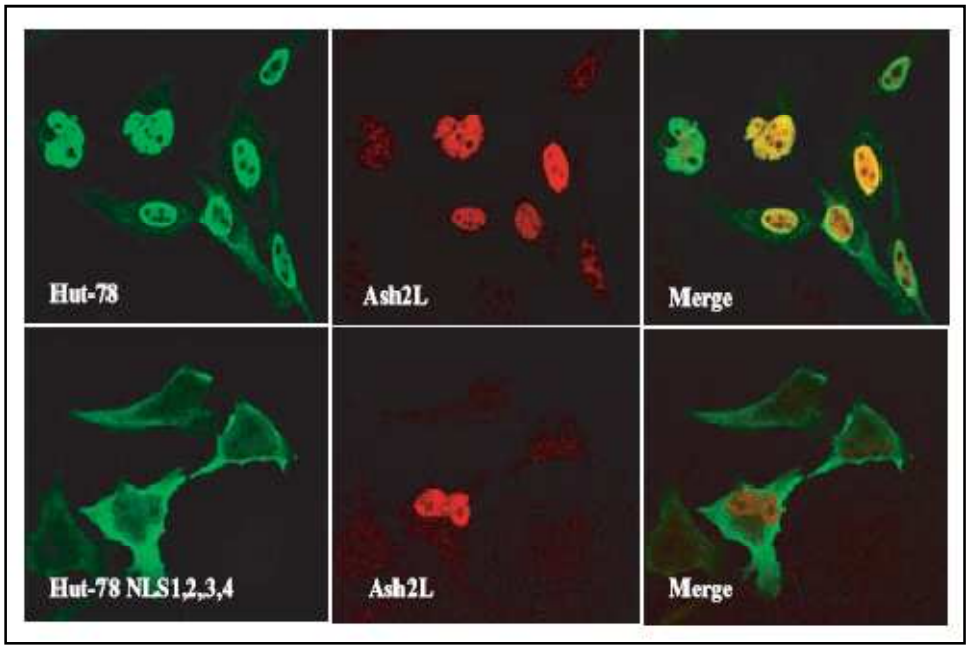

Figure 50: Hut78 but not Hut78 NLS1234 colocalizes with ASH2L in the nucleus. HeLa cells were transfected with the indicated expression plasmids and anti-p100 or -HA immunofluorescences were carried out to detect Hut78, Hut78 NLS1234 or ASH2L, respectively. (Performed with M. Aussems)

To further identify the H3K4 HMT complex recruited by p52 on the *mmp9* promoter, we investigated by ChIP assays, the recruitment of some catalytic H3K4 HMT subunits on the κB-sites of this promoter. We observed that both MLL1 and MLL2 proteins were tethered on the *mmp9* promoter in p52 overexpressing NIH3T3 cells, while we did not find evidence for their recruitment on the *IκBα* promoter (**Figure 51**).

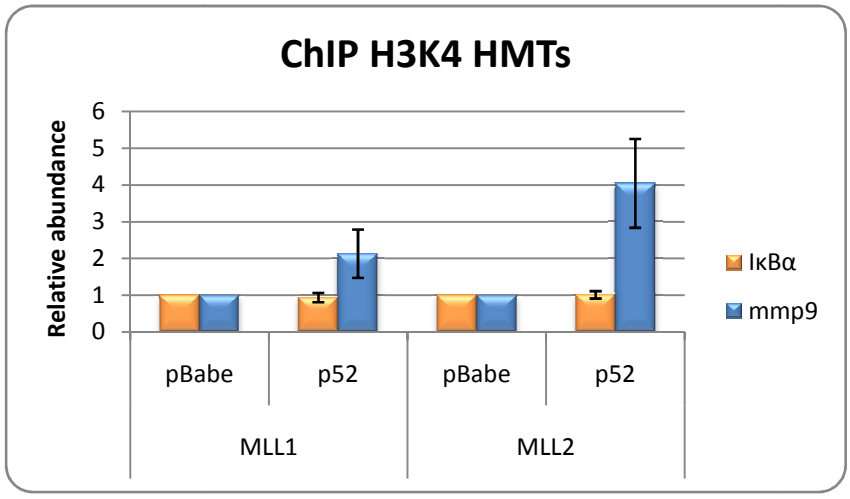

Figure 51: Enhanced MLL1 and MLL2 recruitments to the *mmp9* but not *IκBα* promoter on p52 overexpression in NIH3T3 cells. ChIP assays using an anti-MLL1 or -MLL2 antibody were performed on DNA extracts from NIH3T3 cells infected with the empty pBabe, or the retrovirus expressing p52. The recruitment of MLL1 or MLL2 in the NIH3T3 cells infected with the empty pBabe construct was set to 1 and its levels in the other conditions were relative to that after normalization with H3. The Figure shows the data from three (MLL1) or two (MLL2) independent experiments performed in duplicates (mean values ± S.D).

Therefore, p52 seems to recruit, in a gene-specific manner, two histone H3K4 methyltransferases, namely MLL1 and MLL2, which were shown to display a high degree of similarity and interact with the same cofactors (Ruthenburg *et al*., 2007).